Journal of Materials Chemistry B

Accepted Manuscript

ROYAL SOCIETY OF CHEMISTRY

rsc.li/materials-b

View Article Online
DOI: 10.1039/C7TB01346A

Journal Name

ARTICLE

Synthesis of gold nanoparticles supported on functionalized nanosilica using deep eutectic solvent for electrochemical enzymatic glucose biosensor†

Received 00th January 20xx,
Accepted 00th January 20xx

DOI: 10.1039/x0xx00000x

www.rsc.org/

Siva Kumar-krishnan,[a*] M. Guadalupe-Ferreira García,[a] E. Prokhorov,[b] M. Estevez-González,[a] Ramiro Pérez,[a] Rodrigo Esparza,[a*] and M. Meyyappan.[c]

Engineering the nanoparticle (NP) surface offers an effective approach for the development of enzymatic biosensors or microbial fuel cells with greatly enhanced direct electron transport process. However, lack of control over the surface functioanlization process and the operational instability of the immobilized enzymes are serious issues. Herein, we demonstrate a facile and green deep eutectic solvent (DES) mediated synthetic strategy for efficient amine-surface functionalization of silicon dioxide and to integrate small gold nanoparticles (AuNPs) for glucose biosensor. Owing to the higher viscosity of DES that provides uniform surface functionalization and further coupling of AuNPs on SiO_2 support with improved stability and dispersion. The amine groups of the functionalized Au-SiO_2NPs were covalently linked to the FAD-center of glucose oxidase (GOx) through glutaraldehyde as bifunctional cross-linker, which promotes formation of "electrical wiring" with the immobilized enzymes. The Au-SiO_2NP/GOx/GC electrode exhibits direct electron transfer (DET) for sensing of glucose with a sensitivity of 9.69 µA mM^{-1}, wide linear range from 0.2 to 7 mM and excellent stability. The present green DES-mediated synthetic approach expands the possibilities to support different metal NPs on SiO_2 as a potential platform for biosensor applications.

Introduction

The development of complex nanostructures such as supported metal and metal oxide nanoparticles has attracted continuous research interest for a wide range of applications.[1] Strongly interacting metal oxides with high specific surface area are of interest to finely disperse the active metal nanoparticles owing to their fascinating catalytic activity and ability to promote electron transport through their functional interface.[2,3] Recently, nanostructured silicon dioxide nanoparticles (SiO_2NPs) as host matrix for integrating with different metallic nanoparticles (e.g., Ag, Au, Pt, Pd, or Cu) have enabled nanomaterials with additional functional properties for applications in catalysis,[4] plasmonics,[5] surface enhanced Raman scattering (SERS)[6] and biological applications including stable radiolabling,[7] drug delivery, cancer therapy and multimodal imaging.[8,9] Among others, Au-SiO_2 based nanostructures have been extensively applied for efficient immobilization of biomolecules[10] and biosensing[11] because of their unique surface plasmonic resonance (SPR) properties and high colloidal stability.

Over the past decade, different synthetic strategies have been employed to fabricate Au-SiO_2NPs including thermal annealing,[12] vacuum deposition,[13] self-assembly process[5] and seed-mediated colloidal synthesis.[14–16] One promising approach involves surface functionalizing the SiO_2 support with amine groups by employing (3-aminopropyl) trimethoxysilance (APTES) as silence coupling agent and subsequent chemical reduction of metal ions.[16] However, controlling the homogeneous coupling of smaller metal NPs and finely dispersing them onto the SiO_2 support remains as a great challenge due their high surface energy leading to aggregation and poor attachment to the SiO_2NP surface, resulting in detachment under harsh processing conditions and even vanishing of the supported metal component at ambient-conditions.[17] Hence, it is highly desirable to develop new synthetic approach to support NPs with uniform dispersion and improve their stability. Recently, deep eutectic solvents (DESs) have shown promise as a new class of green solvent alternative to ionic liquids first described by *Abbott* and co-workers in 2003.[18] DESs are generally formed by the self-

[a] *Centro de Física Aplicada y Tecnología Avanzada, Universidad Nacional Autónoma de México, Boulevard Juriquilla 3001, Santiago de Querétaro, Qro., 76230, México. * E-mail: skumar@fata.unam.mx; resparza@fata.unam.mx, Tel: +52-1-5556234173*
[b] *Centro de Investigación y Estudios Avanzados, Unidad Querétaro, Querétaro, Qro., 76230, México.*
[c] *Center for Nanotechnology, NASA Ames Research Center, Moffett Field, Mountain View, California 94035, United States*

† Electronic Supplementary Information (ESI) available: TEM images of Au-SiO_2NPs, XPS survey spectra, Zeta-potential measurements, and Amperometric results. See DOI: 10.1039/x0xx00000x

View Article Online
DOI: 10.1039/C7TB01346A

association of quaternary ammonium salts with hydrogen-bond donors, resulting in a eutectic mixture with melting point below that of the individual constituents.[18,19] Owing to their fascinating properties including nontoxicity, biocompatibility, high chemical stability arising from its polarity and viscosity and extended hydrogen bonded structure, DESs are particularly interesting as sustainable green media for finely dispersing solid nanoparticles and well-controlled surface modification process.[20,21]

Efficient bioelectrocatalytic reactions are of great interest for the fabrication of high performance enzymatic biosensors.[22] Immobilization of enzymes on solid nanoparticles is often considered to be important for improving the surface confined enzymatic reactions, promoting direct electron transfer (DET) process and increasing the operational stability of the biosensor.[22,23] Engineering the NP surface chemistry between the enzyme and the NP surface strongly prevents the inactivation of enzyme catalytic functions which may occur during the direct contact with the native nanoparticle support; it can also significantly enhance the structural flexibility and operational stability of the immobilized enzymes, which result in an improvement in the DET characteristics and the overall efficiency of the biosensor.[23,24] Nanomaterials such as reduced graphene,[25] carbon nanotubes (CNTs),[26] porous carbon,[27] carbon nanodots,[28] metal nanowires,[29] clay based hallow nanotubes,[30] metal organic framework[31] and conducting polymer hydrogels[32] have been extensively exploited for various biomolecule immobilization and promoting the DET process. Among all, silica nanoparticles are particularly promising which combine both high immobilization capacity (more than 90%) and the ability to retain its biocatalytic functions.[33,34] Different strategies have been investigated for integrating the biomolecules with the nanomaterial and to facilitate the DET process.[35] However, the covalent conjugation is perhaps the most powerful immobilization method not only to enhance the stability of the immobilized enzymes but also to promote the DET process instead of direct adsorption of enzymes.[36,37] Incorporation of metal NPs onto the solid support can further enhance the DET process in enzymatic biosensors.[38] In particular, rationally incorporated AuNPs are more efficient for site-specific conjugation and enhancing the charge transport in enzymatic biosensors.[39–41] Synergizing the advantages by combining the high enzyme immobilization capacity of SiO_2NPs and the catalytic properties of AuNPs as efficient nanomaterial for electrically wiring the GOx enzyme is ideal to enhance the charge transport in enzymatic electrochemical glucose detection. To the best of our knowledge, the DES-mediated surface functioanlization, controlled synthesis of Au-SiO_2NPs and DET process on enzymatic biosensing have not been previously investigated.

Herein, we report a facile, non-aqueous phase synthetic approach for surface functioanlization of SiO_2NPs with amine functionality, which allows stable attachment of smaller AuNPs (~5.2 nm) onto the SiO_2NP surface in DES serving as a soft-template. The better dispersibility of SiO_2NPs in a highly viscous DES significantly improves the effectiveness of surface functionalization of NH_2-groups for the incorporation of smaller AuNPs onto the SiO_2 in a well-controlled manner without agglomeration. In addition, we investigate here the potential of surface functionalized Au-SiO_2NPs as electrode material for the redox wiring, which enables FAD-cofactor of the enzyme to be electrically connected to the small AuNPs to promote DET (**Scheme 1**). The rational incorporation of AuNPs on SiO_2NPs support facilitates enhanced charge transport in enzymatic electrochemical glucose biosensor.

Experimental

Materials

Tetraethylorthosilicate (TEOS ≥ 98%), ammonium hydroxide (NH_4OH,28-30%), Gold (III) chloride ($HAuCl_4.4H_2O$, 99.9%), sodium borohydride ($NaBH_4$, ≥99.99%), (3-aminopropyl) triethoxysilane (APTES, 99%), glucose oxidase (GOx, from Aspergillus niger; 15-50K units/g), and D-glucose (≥99.5 %), urea 99%, and choline chloride (ChCl, 98%), methanol (MeOH, 99%), ethanol (EtOH , 90%) were purchased from Sigma-Aldrich. The serum samples were obtained from Instituto Nacional de Rehabilitation (INR) hospital, Mexico City. All reagents were analytical grade and used as received. All glassware was cleaned with deionized water (DI) and air-dried before use in experiments.

Preparation of deep eutectic solvent (DES)

To prepare the DES, choline chloride (ChCl) was first dried at 90ºC in an oven to ensure that ChCl is completely dry. The urea and ChCl were mixed together in a molar ratio of 2:1 and tightly closed and heated in an oven 80°C until a clear, homogeneous liquid was formed. Then, the viscous liquid was cooled to room temperature and saved until later use.

DES-mediated surface modification of Silica NPs and synthesis of Au-SiO_2NPs

Silica nanoparticles with an average diameter of *ca.* 152 nm were prepared following the modified Stöber method reported previously.[42] Briefly, certain quantities of MeOH/EtOH, NH_4OH (20 ml) were mixed in DI water by magnetic stirring for 5 min. Then, 5 ml of TEOS was slowly added to the solution mixture and magnetically stirred for 4 hrs at room temperature. The SiO_2NPs were separated by centrifugation and dried at 120ºC. The resultant sample was washed with DI three times and stored in a humidity-free container until further use. As-prepared template SiO_2NPs were then surface-functionalized with NH_2 groups using APTES in a non-aqueous DES using the protocol reported by Gu *et al.*[43] In a typical process, 10 mg of as-prepared dry SiO_2 NPs were dispersed in 5 ml of DES and then 100 µl of APTES (0.1 mM) was added to the DES-containing SiO_2NPs, and the mixture was magnetically stirred at 60^{o}C overnight to obtain amine (NH_2)-functionalized SiO_2NPs referred as SiO_2-NH_2. After that, 2.5 mg of gold precursor hydrogen tetrachloroaurate (III) ($HAuCl_4.4H_2O$) was added to the amine-functionalized SiO_2NP-DES mixture and magnetically stirred until it is completely dispersed to obtain SiO_2/Au^+ ions mixtures. Then, freshly prepared solutions of

DES-containing sodium borohydride (NaBH4, 1 mg /2ml of DES) was added drop-wise within one minute and stirred at 60°C for 30 min. The color of the reaction mixture turned yellow to dark pink, indicating the reduction of Au^{3+} into Au^0 over the SiO_2NP surfaces referred as Au-SiO_2 NPs. The resultant product was separated from DES by adding equal DI water and centrifugation process. Further, the unreacted Au^{3+} ions and excess borohydride were removed by subsequent washing cycles by DI water three times at 6000 rpm for 15 min and redispersing in DI water.

Enzyme immobilization and Preparation Au@SiO_2-GOx modified electrodes.

For immobilization of glucose oxidase (GOx), 2 mg of as-prepared Au-SiO_2 NPs were used to immobilize GOx through covalent immobilization process. As-synthesized Au-SiO_2 NPs were further amine-functionalized with APTES using similar protocol as the functionalization of SiO_2 NPs. The product was washed twice using DI water in order to remove the excess NH_2 groups on the Au-SiO_2 NPs. After that, 2 mg of NH_2-terminated Au-SiO_2NPs were dispersed in 1 mL of neutral PBS containing 0.2 mL of glutaraldehyde (GA, 50%) as a cross-linker molecule under magnetic stirring for 2 h. The nanoparticles were separated by centrifugation and redispersed in PBS, then added with 0.1 ml of PBS solution (0.1 M) containing GOx (20 mg/mL) and finally incubated overnight for the covalent immobilization of GOx onto the Au-SiO_2NPs. Then the final suspension was dispersed by ultrasonication, and 30 µL of finely dispersed solution was drop casted on the surface of the GCE, and allowed to dry at 4ºC. Finally, the Au-SiO_2/GOx was rinsed with PBS to remove loosely bound GOx and stored at 4ºC in a refrigerator under dry conditions when not in use.

Material characterization

Scanning electron microscopy (SEM) images were obtained from JEOL-JSM7401F field emission scanning electron microscope operating at 20 kV. Scanning transmission electron microscopy (STEM) images were obtained using Jeol JEM-ARM200F STEM/TEM operated at 200 kV. The samples for the STEM measurements were prepared by depositing a drop of the as-prepared SiO_2 and Au-SiO_2 NPs sample on copper grids with carbon film and allowed to dry completely at room temperature. The UV-vis absorption spectra were recorded in an Agilent 8453 UV-vis spectrophotometer (wavelength ranging from 400- 1100 nm). The powder XRD spectra were collected using X-ray diffractometer (Rigaku Ultima IV, using Cu-Kα radiation). Measurements were made using parallel-beam geometry with 2θ scans values from 15 to 80°. The X-ray photoelectron spectra (XPS) results of the samples were obtained in a nonmonochromatic Al Kα (1486.7 eV) X-ray source and a hemispherical electron analyzer with seven channeltrons (model XPS110). All the recorded XPS spectra were corrected utilizing C1s line at 284.8 eV. Infrared transmittance spectra of the dry samples were obtained from a Thermo Scientific (NICOLET 6700) spectrometer, equipped with a universal ATR accessory in the spectral range of 4000-650 cm^{-1}. The N_2-absorption/desorption isotherms were collected utilizing a Belsorp Mini-II sorptometer (BEL, Japan) at 77K after degassing at 180ºC for 8 h.

Electrochemical measurements

The cyclic voltammetry (CV) was performed in a standard three-electrode (VoltaLab 40 PGZ 301) electrochemical cell containing 20 ml of 0.1 M phosphate buffer solution (PBS, pH=7) at room temperature. We used platinum foil as the auxiliary electrode and a saturated calomel electrode (SCE) as the reference one, respectively. Homemade glassy carbon electrodes (GCE, 3 mm diameter) were well polished with 0.3 and 0.05 mm alumina slurries on a polishing paper until reaching a mirror-like surface. This was followed by cleaning the GCE in an ultrasonic bath containing 1:1 water-acetone mixture and then rinsing with DI water and drying in N_2-gas prior to the deposition of the sample. The CV measurements were operated in N_2-saturated, air-equilibrated, and O_2-saturated 0.1M of neutral PBS solution with varying glucose concentrations.

Results and discussion

Synthesis and structural characterization of Au-SiO_2 nanostructures

The Au-SiO_2NPs were prepared *via* a two-step surface modification process. First, monodisperse SiO_2NPs were synthesized using modified Stöber method,[42] followed by functionalizing with amine groups (-NH_2) by mixing certain amount of the particles and APTES in a non-aqueous DES and magnetically stirring at 60°C overnight to promote covalent bonding.[43] The SiO_2 nanoparticles are finely dispersed and stable after 12 hr, whereas in toluene precipitate before 1 hr (Fig S1†). The high viscosity of the DES that confers stability for SiO_2NPs and permits controlled surface functionalization process. In the second step, supporting the AuNPs onto the SiO_2 NPs was accomplished by immobilizing Au^{3+} ions on the NH_2^- modified SiO_2NPs followed by *in-situ* chemical reduction of Au^{3+} to Au^0 using sodium borohydride ($NaBH_4$) for 1 hr at 60°C (Scheme1).

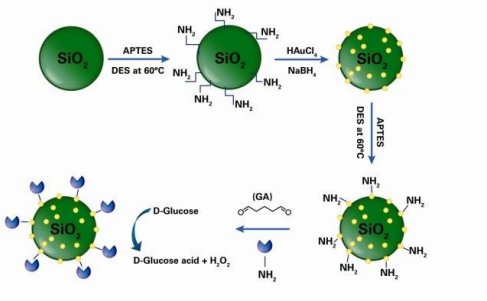

Scheme 1. (a) Schematic illustration displaying the DES-mediated amine-functioanlization of SiO_2NPs (green), which allows stable attachment of small AuNPs (yellow) to obtain Au-SiO_2 NPs and covalent immobilization of glucose oxide (GOx; blue) onto the Au-SiO_2NPs surface.

View Article Online
DOI: 10.1039/C7TB01346A

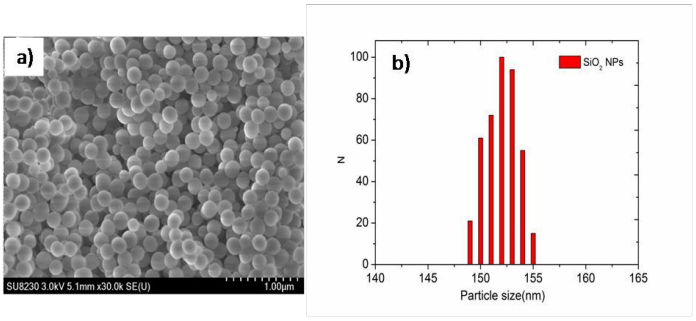

Fig 1. (a) SEM image of as-synthesized SiO_2 nanoparticles, (b) corresponding size-distribution histogram.

Fig. 1 displays the scanning electron microscopy (SEM) images of the bare SiO_2 NPs. Fig. 1a,b shows highly homogeneous spherical SiO_2 NPs with an average diameter of *ca.*152 nm. In addition, transmission electron microscopy (TEM) analysis was performed to characterize the morphology and composition of the as-synthesized Au-SiO_2 NPs. Fig. 2 a, b shows low-resolution TEM images of the as-prepared Au-SiO_2NPs, which confirm the high density of small AuNPs uniformly attached onto the entire surface of SiO_2NPs. The average particles size of the supported AuNPs was calculated to be *ca.*5.2 nm (Fig. S2†). Typical high-resolution (HR-TEM) image of Au-SiO_2NPs indicates that the small crystalline AuNPs are intimately coupled with the SiO_2 surface (Fig. 2c). The calculated lattice spacing of ~2.36 Å is ascribed to the (111) plane of the face centered cubic (fcc) structure of the AuNPs.[3] The number of Au atoms was estimated from the STEM image of a single AuNP (Fig S3†). The result shows that a single particle contains $8.1x10^3$ atoms in which 21% of the atoms are situated on the outer surface of the single Au nanoparticle.

In addition, the elemental distribution of the Au-SiO_2NPs was examined by energy dispersive X-ray spectroscopy (EDX) as presented in Fig. 2d. The EDX-elemental mapping shows SiO_2 nanoparticles (green) located in the core while the Au (red) elements are exclusively seen around the SiO_2NPs, which are homogeneously distributed over the entire surface.

The UV-vis absorption spectra of the as-prepared bare SiO_2 and Au-SiO_2 NPs were recorded after the synthesis process as shown in Fig. 2e**.** No surface plasmon resonance (SPR) peak appears for the template SiO_2 nanoparticles whereas the SPR peak appears at ~529 nm for the Au-SiO_2NPs due to the presence of smaller AuNPs coupled to NH_2-SiO_2NPs.[15,44] As seen in the inset of Fig. 2e, the formation of metallic AuNPs on the NH_2-SiO_2 is clearly perceptible by the color change of the particle solution from white to deep red color. Notably, the resultant nanoparticles are highly stable, which is conferred by the high viscosity of DES. The powder X-ray diffraction (pXRD) pattern of the bare SiO_2 and Au-SiO_2NPs (Fig. 2f) show the appearance of weak diffraction peak which can be indexed to the amorphous phase of SiO_2NPs; the four well-resolved diffraction peaks at 38, 44.4, 64.6 and 77.7 degrees correspond to the planes (111), (200), (220) and (311) respectively of face-centered cubic (fcc) structure of metallic AuNPs (JCPDS card no. 19-0629).[15]

The surface functionalization and the chemical state of the Au-SiO_2NPs was further examined by X-ray photoelectron spectroscopy (XPS) analysis. The XPS survey scan for the Au-SiO_2NPs reveals the presence of Si, O, N, Au and C peaks (Fig. S4†). In the N 1s region, the spectrum was fitted using two singlets centered at 400.10 and 402.73 eV (Fig. 3a), which are mainly associated with the presence of amine (NH_2) functionality on the surface, as a result of successful

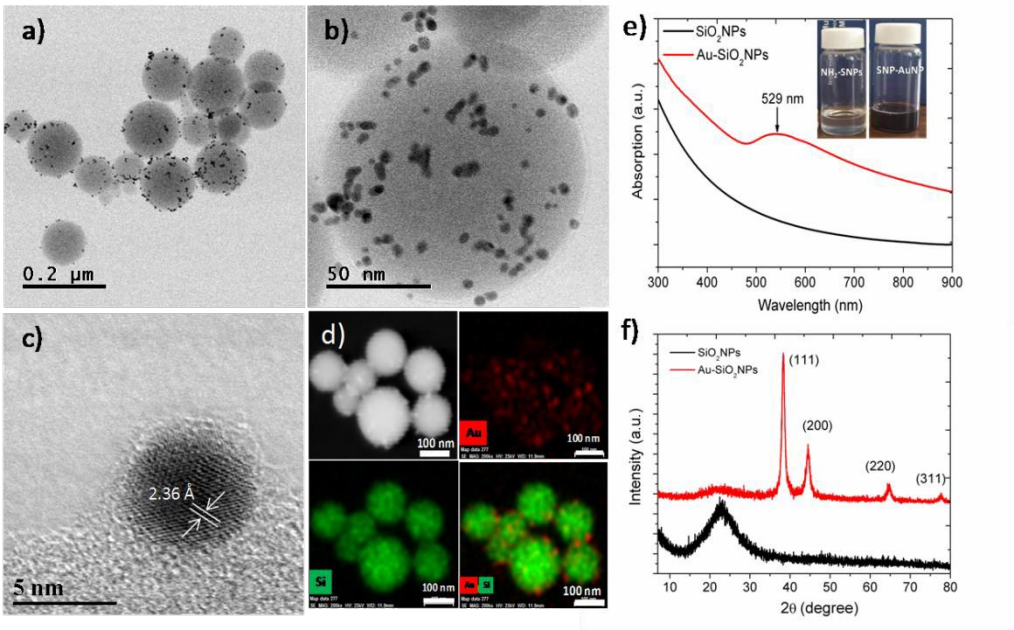

Fig 2. TEM images of (a, b) AuNPs supported SiO_2NPs. (c) HR-TEM images of the single AuNPs, and d) HAADF-STEM image and corresponding EDX-elemental mapping of the Au-SiO_2NPs showing Au elements (red), Si (green) and overlapped (red+green).(e) UV-vis absorption spectra of as-prepared SiO_2NPs and Au-SiO_2 NPs in DES. The inset shows a photograph of the corresponding nanoparticles. (f) X-ray diffraction (XRD) pattern of bare SiO_2 NPs and Au-SiO_2 NPs.

functionalization of SiO_2 with NH_2 groups.[45] Fig. 3b shows the high-resolution XPS spectrum of Si 2P region with the peak centered at 103.13 eV related to Si^{4+} from the oxide nanoparticles. The Au 4f core-levels were fitted using two doublets with a spin-orbit separation of 3.66 eV (Fig. 3c). The first doublet centered at 83.6 eV is associated with Au^0 while the second one centered at 85.35 eV is associated with Au^{3+}, respecgtively.[46,47] The specific surface area (SSA), and mean pore diameter of the SiO_2 and Au-SiO_2NPs were measured using the well-known Bruner-Emmett-Teller (BET) method.[48] The N_2 adsorption/desorption measurements on bare and functionalized NPs show typical hysteresis loops of porous feature (Fig. 3d). Interestingly, compared with the bare SiO_2NPs, the BET surface area and pore diameter of Au-SiO_2 NPs are increased: SSA from 25.58 m^2g^{-1} to 32.1 m^2g^{-1} and the average pore diameter from 47.03 to 81.49 nm, respectively (Inset of Fig. 3d). The significant increase in the pore size may result from the strong coupling of the surface bounded smaller AuNPs onto SiO_2 surface, significant decrease in the surface roughness[49] and formation of small cavities between two nearby NPs.[38] As a result, the average pore size is increased.

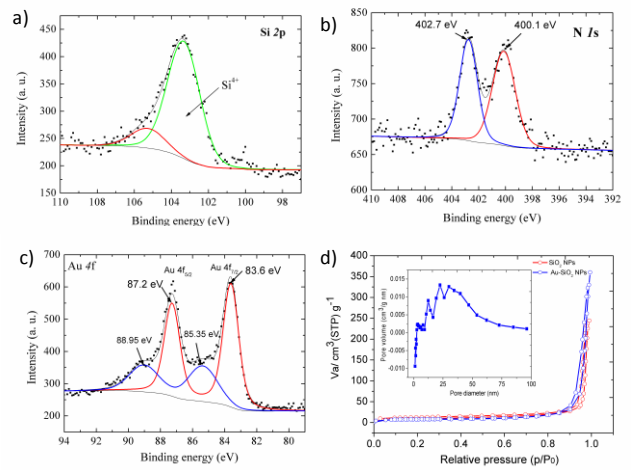

Fig 3. Structural characterization of Au-SiO_2 NPs. (a-c) Core-level XPs spectra of Si 2p (a), N 1s (b), and Au 4f (c) spectra for the Au-SiO_2 NPs. (d) N_2 absorption-desorption isotherms of the SiO_2 and Au-SiO_2NPs. The inset in (d) shows the pore-size distribution of the Au-SiO_2NPs.

Covalent immobilization of GOx and characterization

The covalent immobilization of GOx enzymes onto the Au-SiO_2NPs was achieved by further surface functionalization with APTES to provide surface exposed -NH_2 groups on the surface and then covalent conjugation *via* glutaraldehyde (GA) as bifunctional cross-linker molecule (Scheme 1).[50,51] Specifically, the NH_2 exposed surface was reacted with the GA molecules, thereby forming C-N bond between NH_2 exposed Au-SiO_2NPs and on the other end linking with the GOx containing-NH_2 groups.[52] The covalent conjugation can lead to connecting AuNPs with the FAD co-factor unit of GOx, which serves as a "bridge" to enhance the charge transport during the enzymatic

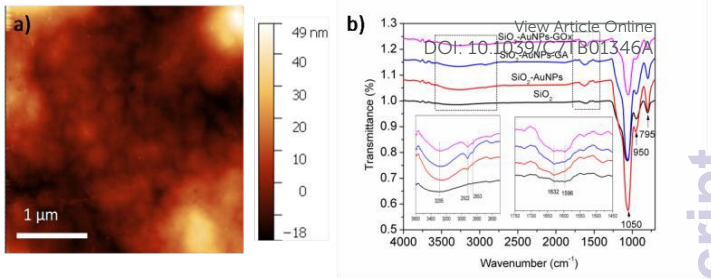

Fig 4. (a) AFM image showing covalently immobilized GOx enzyme to the amine functionalized AuNPs-SiO_2NPs *via* glutaraldehyde (GA) cross-linker molecule. (b) FT-IR spectra of bare SiO_2 and Au-SiO_2NPs with varied surface functionalization steps as indicated. Inset showing magnified spectra from the marked region.

reaction.[38,51] Fig. 4a shows the atomic force microscopy (AFM) topographical image after attachment of GOx onto Au-supported SiO_2NPs. As seen from Fig. 4a, the GOx enzymes are attached on the surface of the amine-modified Au-SiO_2NPs, suggesting a good binding affinity. Further, we carried out Fourier transform infrared spectroscopy (FT-IR) presented in Fig. 4b to confirm the surface functionalization and covalent-conjugation of GOx enzymes. The FT-IR peaks of the bare SiO_2 are sharp centered at 950 cm^{-1} associated to the asymmetric vibration of Si-OH and at 795 and 1050 cm^{-1} associated with symmetric and asymmetric vibrations of Si-O, respectively.[50] After surface functionalization of SiO_2 and Au-SiO_2NPs with APTES in DES at 60º C, the small increase in the peak intensity at 1596 cm^{-1} corresponds to N-H bond in the primary amines. Additionally, a peak at 3295 cm^{-1} and two additional peaks at 2922 and 2853 cm^{-1} newly appear which are assigned to the stretching vibration of N-H, and C-H asymmetric and symmetric stretching vibrations of APTES, respectively.[53] Upon covalent immobilization of GOx enzymes *via* GA cross-linker molecule, the peak intensity at 1632 cm^{-1} significantly increases compared to the Au-SiO_2NP peaks; the additional peak at 1596 cm^{-1} is assigned to the stretching vibration of C-N linkage, suggesting covalent-conjugation between the enzyme and the surface exposed NH_2 groups.[29, 50, 52] In addition to the FT-IR spectra, zeta-potential measurements are in good agreement with the surface functionalization steps (Table S1). The bare SiO_2NPs exhibit negative surface charge (-38.62±1 mV), which turn into positive value of 24.9±0.5 mV after the surface modification with amine groups. The AuNPs-supported SiO_2NPs show decreases in the surface charge from 24.9±0.5 mV to 1.37±0.8 mV. This significant reduction in the surface charge indicates that the most of the amine groups are attached to the AuNPs. Upon immobilization of GOx to the Au-SiO_2NPs, the zeta-potential value is inverted again to -4.24±0.4 mV arising from the slightly negative charge of the GOx enzymes. This surface-charge difference for the surface modification steps is consistent with previous reports.[50] These results unambiguously confirm the covalent coupling of GOx enzyme on the Au-SiO_2NPs surface.

View Article Online
DOI: 10.1039/C7TB01346A

DET of Au-SiO_2NPs/GOx-modified GCE electrode

The GOx functionalized Au-SiO_2NP-modified glassy carbon electrode (GCE) was used as working electrode in testing for DET in electrochemical sensing of glucose. The amperometric glucose detection was studied using cyclic voltammetry (CV) in a phosphate buffer solution (PBS). Fig. 5 compares the CVs for different electrodes such as the bare GCE, SiO_2NP/GCE, Au-SiO_2NP/GCE, Au-SiO_2NP-GOx/GCE and covalently functionalized Au-SiO_2NP-GOx/GCE electrodes in N_2-saturated (PBS, pH 7.4). The CV results indicate that the bare GCE, SiO_2NP/GCE and Au-SiO_2NP/GCE do not show any redox peaks in the interested potential range in the CV cycle, whereas the Au-SiO_2NPs/GOx/GCE shows two well-defined redox peaks of cathodic (E_{pc}) peak potential at -0.49 V and anodic (E_{pa}) peak potential of -0.42 V, respectively. The observed redox peaks are associated to the standard oxidation and reduction potential values of FAD/$FADH_2$ of GOx in a neutral solution.[54] The CV curve for the covalently functionalized GOx in Fig. 5 displays a significant increase in intensity as well as slight negative-shift. These changes are due to the APTES-functionalized Au-SiO_2NP surface effectively linked to the FAD-active sites of GOx through the GA cross-linker, resulting in decrease in the distance between the FAD-GOx and the electrode surface and enhancement in the charge transport.[51] This result indicates that the FAD-GOx on the Au-SiO_2NP/GOx/GC electrode undergoes quasi-reversible redox reaction and can promote the DET process between the GOx and the electrode surface.

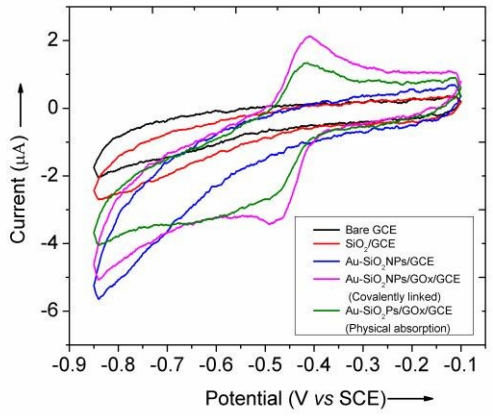

Fig 5. The comparison of CV curves for different modified electrodes measured in N_2-saturated PBS (pH= 7.4) at a scan rate of 50 mVs^{-1}.

The DET process can be described by the following expression.[37,55]

D-glucose + GOx (FAD) → *D*-glucono-1,5-lactone + GOx ($FADH_2$), (1)

GOx ($FADH_2$) → GOx (FAD) + $2H^+$ +2*e*- (2)

Where, FAD and $FADH_2$ are the oxidized and reduced forms of the redox center of GOx enzyme. It is well known that the GOx is a homodimer containing its cofactor (FAD) bound to its two identical 80-kDa subunits, which can easily undergo enzymatic reaction upon addition of glucose.[56] Upon introduction of glucose, the FAD center of the GOx reacts with D-glucose and converts into D-glucono-1-5-lactone and two protons and two electrons are transferred from the glucose to FAD, which reduces into $FADH_2$. Subsequently, the $FADH_2$ can oxidize back to FAD in the absence of oxygen or electrochemical mediators, typically referred as the occurrence of DET.[51]

The electroactive enzyme surface density (Γ, mol/ cm^2) on the modified electrode was evaluated according to the following expression:[57]

$$\Gamma = Q/nFA \quad (3)$$

Where, Q is the charge involved in the reaction (obtained by integrating the anodic peak and dividing by the scan rate of 50 mVs^{-1}), n is the number of transferred electrons (n = 2), F is the Faraday constant and A is the geometric area of the GCE electrode used (0.07 cm^{-2}). The estimated immobilized enzyme coverage *via* simple physical adsorption and covalent-conjugation on the electrode is $7.94x10^{-8}$ mol/ cm^2 and $8.65x10^{-8}$ mol/ cm^2, respectively. The covalent linkage improves the enzyme coverage, and the value is higher than the previously reported value for covalent conjugation with AuNPs supported on the M13 Bacteriophage ($4.74x10^{-8}$ mol/cm^2),[58] hierarchical 1-D TiO_2 nanostructures ($6.8x10^{-10}$ mol/cm^2)[54] and pyrroloquinoquinone (PQQ)/GOx ($1.7 x10^{-12}$ mol/cm^2).[59]

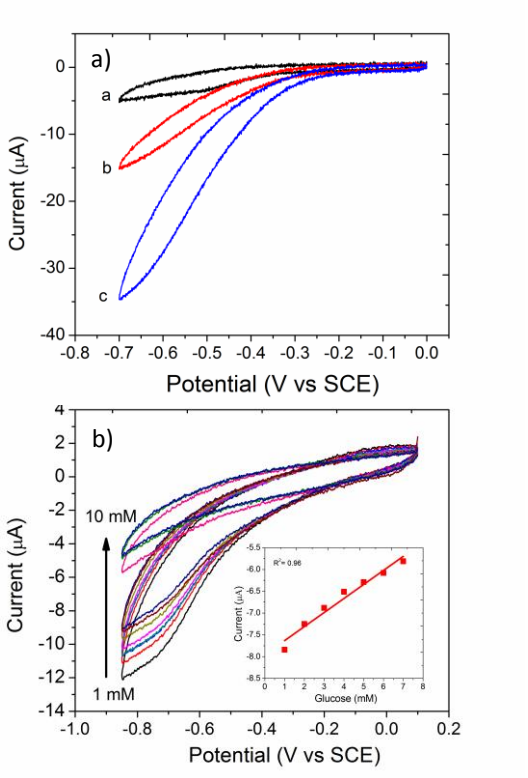

Fig 6. (a) CVs of AuNPs-SiO_2/GOx-GC electrode measured with (a) N_2-saturated, (b) air-saturated, and (c) O_2-saturated 0.1 M of neutral PBS solution. (b) CVs of the Au-SiO_2NPs/GOx/GC electrode operated in air-equilibrated neutral PBS with increasing glucose concentration (1-10 mM) at a sweep rate: 50 mVs^{-1}.

View Article Online
DOI: 10.1039/C7TB01346A

This significant enhancement in the enzyme surface coverage may result from the combined effect of both effective covalent linkage of GOx on the high-surface area template SiO_2NPs and supported AuNPs on the SiO_2NP template which further enhances the active surface area.[60]

Fig. 6a compares the CVs of an Au-SiO_2NPs/GOx-GC electrode in N_2-saturated, air-equilibrated, and O_2-saturated PBS solutions. In the N_2-saturated condition, a pair of redox peaks originated from the FAD/$FADH_2$ is seen (Fig. 6a, line a). In the air-equilibrated solution, a significant increment in the cathodic peak current but a decrease in the anodic current is observed (Fig. 6a, line b) due to the reduction of dissolved O_2 and the redox FAD for yielding $FADH_2$. In addition, the reduction current is higher in O_2-saturated solution compared with the N_2-saturated, and air-saturated solutions (Fig. 6a, line c). Such high reduction current could arise from the higher amount of dissolved O_2- in the PBS solution that will compete with the oxidation reaction occurring for $FADH_2$ by oxygen.[26,51] To study the direct electron transfer process of the Au-SiO_2/GOx/GC electrode, we measured CVs with different concentrations of glucose in both air-equilibrated and O_2-saturated PBS solutions. Fig. 6b shows the CVs of an Au-SiO_2NP/GOx/GC electrode in air-saturated condition for glucose concentration from 1 to 10 mM where the cathodic reduction peak current decreases and reaches saturation. The respective calibration plot (inset of Fig. 6b) exhibits a linear range between 1-7 mM and saturates after 7 mM.

Fig. 7a depicts the CV in oxygen-saturated 0.1 M neutral PBS solution at a scan rate of 50 mVs^{-1} for various concentrations of glucose. The reduction current gradually decreases upon increasing the glucose concentration glucose and exhibits a linear relationship in the concentration range of 0.2-8 mM (Inset in Fig.7a) and then reaches saturation. The linear decrease in the cathodic current for different glucose concentrations arises from the electrocatalytic reduction of the FAD in the modified electrode by dissolved oxygen.[54] The sensitivity of the biosensor is estimated to be 9.69µA $mM^{-1}cm^{-2}$. The sensitivity and the linear range of the biosensor exceed those of most other nanomaterial based DET systems for detecting glucose as presented in Table 1**.** Such sensitivity enhancement can be attributed not only due to the excellent immobilization capacity of the SiO_2NP support and electrocatalytic properties of the supported AuNPs but also due to the site-specific conjugation of GOx, resulting in "electrical wiring" of the FAD-cofactor in GOx through the AuNPs. Consequently, the electrically interconnected networks serve as an electrical bridge to make the electron transport more efficient. Furthermore, the amperometric response of the Au-SiO_2NPs/GOx/GC electrode with successive injection of 1 mM of glucose (Fig. S5a†). No changes in the reduction current for the SiO_2NP/GOx-GC electrode is seen, whereas the electrode constructed using Au-SiO_2NP/GOx/GC electrodes shows clear changes upon each addition of 1 mM of glucose. Notably, the response in the reduction current is at the low glucose concentrations ranging from 0.2 mM-1.5 mM (Fig. S5b†).

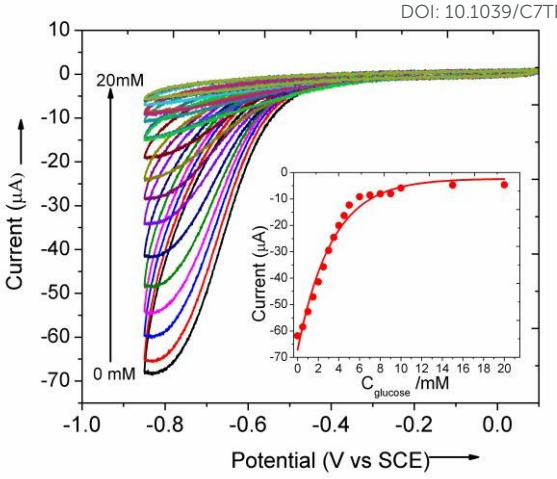

Fig 7. CVs of the Au-SiO_2/GOx/GCE modified electrode with various glucose concentrations in 0.1 M of PBS under O_2-saturated condition. Scan rate 50 mVs^{-1}. inset showing the current-glucose concentration calibration plot.

To further validate the AuNP-mediated electron transfer, we conducted a control experiment by varying the concentration of supported AuNPs on SiO_2NPs. TEM images show that the attachment of AuNPs on SiO_2NPs has a linearly dependence on the Au precursor concentration in the DES (Fig. S6†). Fig. 8a shows the sensitivity of the Ag-SiO_2NP/GOx-GC electrodes as a function of AuNP loading. The sensitivity increases linearly with the AuNP loading from 8.23 to 20.89 µA mM^{-1} (from 0.25 to 2 mg of AuNP loading). The sensitivity is low at low AuNP concentrations due to the limited availability of AuNPs that are conjugated with the FAD-unit of the GOx. The sensitivity reaches a maximum at higher AuNP loading of 20.89 µA at 2 mg. Interestingly, at higher AuNP concentrations, the immobilized GOx are effectively contacted through AuNPs, and thus the sensitivity is significantly enhanced. In addition, previous studies[31,61] have shown that the sensitivity of the biosensor also depends on the immobilized GOx fraction. Thus, we evaluated the biosensor performance by varying immobilized GOx concentration. Fig. 8b, shows that the sensitivity increases with GOx concentration until 20 mg/ ml, peaking at 12.76 µA mM^{-1}. Interestingly, the sensitivity drops above 20 mg/ ml. This phenomenon is because there are limited covalently conjugated GOx at low GOx concentrations that are involved in the enzymatic reaction. At higher concentrations (above 20 mg/ml), significantly higher GOx imposes steric hindrances between adjacent GOx molecules at the curved Au-SiO_2NP surfaces and partial GOx bound through physical adsorption. This is confirmed by the appearance of reduction peak in the redox potential at 0.25 V vs. SCE reference electrode (Fig. S7†), associated with the redox potential of free GOx.[26] This result is consistent with our the previous study,[29] where the sensitivity drastically drops for GOx concentrations above ~20-30 mg/ml. Overall, these results confirm the DET mechanism in the Au-SiO_2NPs/GOx/GC electrode and importance of the surface-supported AuNPs in

achieving electrically favorable enzyme/nanoparticle interface for efficient direct electron transfer.

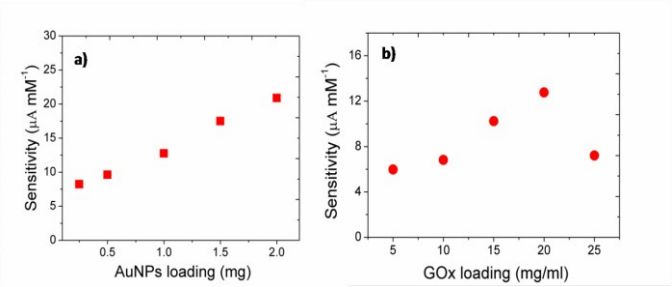

Fig 8. (a) Dependencies of sensitivity for glucose detection by varying the AuNPs loading onto SiO_2NPs support, and (b) concentration of immobilized GOx, respectively.

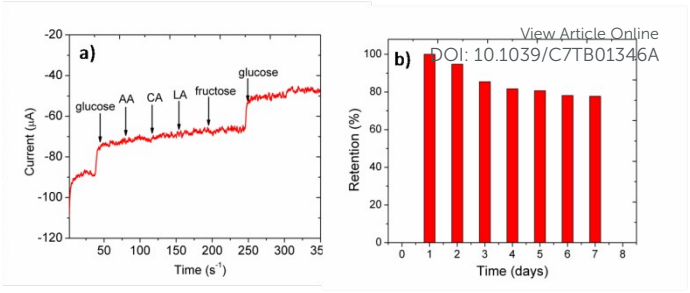

Fig 9. (a) Amperometric response of Au-SiO_2NPs/GOx-GC electrode to 1 mM of glucose and in the presence of different interfering substances such as 0.3 mM AA, 0.5 mM CA, 0.5 mM LA, and 0.5 mM of fructose at -0.5 V. (b) Stability of the Au-SiO_2NPs/GOx-GCE for a week-long period.

Interference, stability and serum sample analysis

The Au-SiO_2NPs/GOx/GC electrode exhibits excellent selectivity toward glucose detection. Fig. 9a shows the effect of most common interfering species such as ascorbic acid (AA), citric acid (CA), lactic acid (LA), and fructose. Addition of different interfering substances (0.5 mM of AA, 0.3 mM of CA, 0.3 mM of LA, and 0.5 mM of fructose) does not show any changes in the reduction current, whereas an apparent change in the current upon introduction of 1 mM of glucose into the solution is seen, suggesting excellent selectivity of the biosensor. This effect is mainly due to the enzymatic reaction occurring selectively between the immobilized GOx and the glucose resulting in two electrons being directly transferred to the electrode surface. Furthermore, we evaluated the stability of the biosensor for a one-week period (Fig. 9b) and the sensor retained about 79 % of its original response and exhibited almost the same reduction current with identical conditions after one week, suggesting excellent stability for practical applications. Finally, to investigate the suitability of the biosensor in real samples, we evaluated glucose detection in human serum. For detection

Table 1. Comparison of analytical performance of different metal nanoparticles based enzyme electrodes for electrochemical glucose biosensor.[a]

electrodes	sensitivity ($\mu A\ cm^{-2}\ mM^{-1}$)	detection limit (μM)	linear range (mM)	ref
CNDs/GOx	6.28	1.07	0-0.64	28
Nafion/GOx-X-APTES/BDD	-	30	0.035-8	51
DMIm/Au_{25}/GOx	0.21	-	1-6	61
1-D TiO_2/GOx	9.9	-	0.2-1	54
PMA/diamond/GOx	0.006	1	0-3	62
GR/CNT/ZnONPs/GOx	5.36	4.5	0.01-6.5	63
HNT/AgNPs/GOx	5.2	-	0.2-6	45
CS/Pd@Pt NC/GOx	6.82	0.2	1-6	64
SiO_2/AuNPs/GOx	9.69	0.2	0.2-7	this work

[a]BDD: boron-doped diamond; CNDs: carbon nanodots, DMI: 1-decyl-3-methylimidazolium; TiO_2: Titanium dioxide; PMA: poly (methacrylic acid); GR: graphene; CNT: carbon nanotubes; HNT: holloysite nanotubes.

View Article Online
DOI: 10.1039/C7TB01546A

of glucose in human serum samples, first the standard glucose (1mM) was introduced, followed by addition of human serum (50 μL), and again with 1mM of glucose were subjected (Figure S8†). The results showed that the response signal was slightly less compared than that of standard glucose due to the matrix effect caused by human serum. The recovery rate of the glucose for the second injection is about 85 %, demonstrating that the modified electrode can be apply to determine the glucose level in human serum.

Conclusions

We have described a simple and green synthetic strategy for the preparation of Au-SiO_2 NPs in a non-aqueous DES. We have systematically investigated the effect of surface modification and immobilization of GOx enzyme with the Au-SiO_2NPs *via* covalent linkage and implemented the strategy for glucose biosensing. The fabricated modified electrode based on Au-SiO_2NPs/GOx/GC electrode can promote DET and yield excellent glucose sensing performance such as high sensitivity, wide linear range and high specificity. The enhanced charge transfer is due to the site-specific conjugation of the enzyme leading to efficient electrical wiring between small AuNPs and the FAD-co-factor unit as a "bridge" resulting in significantly improved charge transfer between the enzyme and the electrode surface. The present green approach for the preparation of AuNPs on the SiO_2NP surface and surface modification for electrically wiring the biomolecules represent a promising strategy for potential applications in mediator-free third generation enzymatic biosensors or enzyme-based biofuel cells.

Acknowledgements

The authors acknowledge PAPIIT-DGAPA for financial support with grant IN113317. Also, Dra. Genoveva Hernandez for the SERS measurements and Ma. Lourdes Palma Tirado (Campus UNAM Juriquilla, Qro) for TEM measurements, and Dr. U. Pal for BET measurements.

Notes and references

1 H. Tang, J. Wei, F. Liu, B. Qiao, X. Pan, L. Li, J. Liu, J. Wang and T. Zhang, *J. Am. Chem. Soc.*, 2016, **138**, 56–59.
2 G. Pacchioni, *Phys. Chem. Chem. Phys.*, 2013, **15**, 1737–1757.
3 J. Fang, Y. Zhang, Y. Zhou, S. Zhao, C. Zhang, H. Zhang, X. Sheng and K. Wang, *Langmuir*, 2017, **33**, 2698–2708.
4 P. Lu, C. T. Campbell and Y. Xia, *Nano Lett.*, 2013, **13**, 4957–4962.
5 M. D. Mcconnell, M. J. Kraeutler, S. Yang and R. J. Composto, *Nano Lett.*, 2010, **10**, 603–609.
6 Y. Shin, J. Song, D. Kim and T. Kang, *Adv. Mater.*, 2015, **27**, 4344–4350.
7 T. M. Shaffer, S. Harmsen, E. Khwaja, M. F. Kircher, C. M. Drain and J. Grimm, *Nano Lett.*, 2016, **16**, 5601–5604.
8 M. Hembury, C. Chiappini, S. Bertazzo, T. L. Kalber and G. L. Drisko, *Proc. Natl. Acad. Sci.*, 2015, **12**, 1959–1964.
9 A. H. Mo, P. Landon, K. Santacruz Gomez, H. Kang, J. Lee, C. Zhang, W. Janetanakit, V. Sant, T. Lu, D. A. Colburn, S. Akkiraju, S. Dossou, Y. Cao, K. Lee, S. Varghese, G. Glinsky and R. Lal, *Nanoscale*, 2016, **8**, 11840–11850.
10 E. Briand, V. Humblot, J. Landoulsi, S. Petronis, C. M. Pradier, B. Kasemo and S. Svedhem, *Langmuir*, 2011, **27**, 678–685.
11 M. You, S. Yang, W. Tang, F. Zhang and P.-G. He, *ACS Appl. Mater. Interfaces*, 2017, **9**, 13855–13864.
12 Y. Lu, H. Xiong, X. Jiang, Y. Xia, M. Prentiss and G. M. Whitesides, *J. Am. Chem. Soc.*, 2003, **125**, 12724–12725.
13 S. Fujii, Y. Yokoyama, Y. Miyanari, T. Shiono, M. Ito, S. I. Yusa and Y. Nakamura, *Langmuir*, 2013, **29**, 5457–5465.
14 R. Wang, X. Ji, Z. Huang, Y. Xue, D. Wang and W. Yang, *J. Phys. Chem. C*, 2016, **120**, 377–385.
15 D. Shao, H. Sun, M. Yu, J. Lian and S. Sawyer, *Nano Lett.*, 2012, **12**, 5840–5844.
16 S. Fazzini, M. C. Cassani, B. Ballarin, E. Boanini, J. S. Girardon, A.-S. Mamede, A. Mignani and D. Nanni, *J. Phys. Chem. C*, 2014, **118**, 24538–24547.
17 D. Kim, N. Becknell, Y. Yu and P. Yang, *Nano Lett.*, 2017, **17**, 2732–2737.
18 A. P. Abbott, D. Boothby, G. Capper, D. L. Davies and R. Rasheed, *J. Am. Chem. Soc*, 2004, **126**, 9142-9147.
19 Q. Zhang, K. De Oliveira Vigier, S. Royer and F. Jérôme, *Chem. Soc. Rev.*, 2012, **41**, 7108–7146.
20 D. V Wagle, H. Zhao and G. a Baker, *Acc. Chem. Res.*, 2014, **47**, 2299–2308.
21 J. Zhang, T. Wu, S. Chen, P. Feng and X. Bu, *Angew. Chemie - Int. Ed.*, 2009, **48**, 3486–3490.
22 A. Küchler, M. Yoshimoto, S. Luginbühl, F. Mavelli and P. Walde, *Nat. Nanotechnol.*, 2016, **11**, 409–420.
23 S. K. Vashist, E. Lam, S. Hrapovic, K. B. Male and J. H. T. Luong, *Chem. Rev.*, 2014, **114**, 11083–11130.
24 E. Tellechea, K. J. Wilson, E. Bravo and K. Hamad-Schifferli, *Langmuir*, 2012, **28**, 5190–5200.
25 G. Bharath, R. Madhu, S.-M. Chen, V. Veeramani, a. Balamurugan, D. Mangalaraj, C. Viswanathan and N. Ponpandian, *J. Mater. Chem. B*, 2015, **3**, 1360–1370.
26 M. Wooten, S. Karra, M. Zhang and W. Gorski, *Anal. Chem.*, 2013, **86**, 752–757.
27 S. Tsujimura, K. Murata and W. Akatsuka, *J. Am. Chem. Soc.*, 2014, **136**, 14432–14437.
28 M. Zhao, Y. Gao, J. Sun and F. Gao, *Anal. Chem.*, 2015, **87**, 2615–2622.
29 S. Kumar-Krishnan, S. Chakaravarthy, A. Hernandez-Rangel, E. Prokhorov, G. Luna-Bárcenas, R. Esparza and M. Meyyappan, *RSC Adv.*, 2016, **6**, 20102–20108.
30 C. Chao, J. Liu, J. Wang, Y. Zhang, B. Zhang, Y. Zhang, X. Xiang and R. Chen, *ACS Appl. Mater. Interfaces*, 2013, **5**, 10559–10564.
31 S. Patra, T. Hidalgo-Crespo, A. Permyakova, C. Sicard, C. Serre, A. Chausse, N. Steunou and L. Legrand, *J. Mater. Chem. B*, 2015, **3**, 8983–8992.
32 L. Li, Y. Shi, L. Pan, Y. Shi and G. Yu, *J. Mater. Chem. B*, 2015, **3**, 2920–2930.
33 H. R. Luckarift, J. C. Spain, R. R. Naik and M. O. Stone, *Nat. Biotechnol.*, 2004, **22**, 211–213.
34 H. Gustafsson, A. Küchler, K. Holmberg and P. Walde, *J. Mater. Chem. B*, 2015, **3**, 6174–6184.
35 K. E. Sapsford, W. R. Algar, L. Berti, K. B. Gemmill, B. J. Casey, E. Oh, M. H. Stewart and I. L. Medintz, *Chem. Rev.*, 2013, **113**, 1904–2074.
36 P. Asuri, S. S. Bale, R. C. Pangule, D. a. Shah, R. S. Kane and J. S. Dordick, *Langmuir*, 2007, **23**, 12318–12321.
37 J. M. Goran, S. M. Mantilla and K. J. Stevenson, *Anal. Chem.*, 2013, **85**, 1571–1581.
38 A. Trifonov, R. Tel-Vered, M. Fadeev, A. Cecconello and I. Willner, *Electroanalysis*, 2015, **27**, 2150–2157.

39 O. Yehezkeli, R. Tel-Vered, S. Raichlin and I. Willner, *ACS Nano*, 2011, **5**, 2385–2391.
40 Y. Xiao, F. Patolsky, E. Katz, J. F. Hainfeld and I. Willner, *Science*, 2003, **299**, 1877–1881.
41 J. T. Holland, C. Lau, S. Brozik, P. Atanassov and S. Banta, *J. Am. Chem. Soc.*, 2011, **133**, 19262–19265.
42 G. Ferreira, A. R. Hernandez-Martinez, H. Pool, G. Molina, M. Cruz-Soto, G. Luna-Barcenas and M. Estevez, *Mater. Sci. Eng. C*, 2015, **57**, 49–57.
43 T. Gu, M. Zhang, J. Chen and H. Qiu, *Chem. Commun.*, 2015, **51**, 9825–9828.
44 L. Latterini, L. Tarpani, D. Chimica, M. Innovativi and V. Elce, *J. Phys. Chem. C*, 2011, **115**, 21098–21104.
45 S. Kumar-krishnan, U. Pal, E. Prokhorov, O. A. De Fuentes, R. Esparza and M. Meyyappan, *J. Mater. Chem. B*, 2016, **4**, 2553–2560.
46 M. P. Casaletto, A. Longo, A. Martorana, A. Prestianni and A. M. Venezia, *Surf. Interface Anal.*, 2006, **38**, 1380–1385.
47 S. K. Maji, S. Sreejith, A. K. Mandal, X. Ma and Y. Zhao, *ACS Appl. Mater. Interfaces*, 2014, **6**, 13648–56.
48 S. Brunauer, L. S. Deming, W. E. Deming and E. Teller, *J. Am. Chem. Soc.*, 1940, **62**, 1723–1732.
49 M. Kamp, M. Hermes, C. M. Van Kats, D. J. Kraft, W. K. Kegel, M. Dijkstra and A. Van Blaaderen, *Langmuir*, 2016, **32**, 1233–1240.
50 X. Ma, A. Jannasch, U.-R. Albrecht, K. Hahn, A. Miguel-López, E. Schäffer and S. Sánchez, *Nano Lett.*, 2015, **15**, 7043–7050.
51 Y. F. Bai, T. Bin Xu, J. H. T. Luong and H. F. Cui, *Anal. Chem.*, 2014, **86**, 4910–4918.
52 L. Li, Y. Wang, L. Pan, Y. Shi, W. Cheng, Y. Shi and G. Yu, *Nano Lett.*, 2015, **15**, 1146–1151.
53 M. Zou, M. Du, H. Zhu and C. Xu, *J Phys.DAppl.Phys*, 2012, **325302**, 325302–325309.
54 P. Si, S. Ding, J. Yuan, X. W. Lou and D. H. Kim, *ACS Nano*, 2011, **5**, 7617–7626.
55 . Lee, H. Ahn, I. Choi, M. Boese and M. J. Park, *Macromolecules*, 2012, **45**, 3121–3128.
56 R. A. S. Nascimento, R. E. Özel, W. H. Mak, M. Mulato, B. Singaram and N. Pourmand, *Nano Lett.*, 2016, **16**, 1194–1200.
57 J. F. Rusling and R. J. Forster, *J. Colloid Interface Sci.*, 2003, **262**, 1–15.
58 R. A. Blaik, E. Lan, Y. Huang and B. Dunn, *ACS Nano*, 2016, **10**, 324–332.
59 E. Katz, A. Riklin, V. Heleg-Shabtai, I. Willner and A. F. Bückmann, *Anal. Chim. Acta*, 1999, **385**, 45–58.
60 S. L. Young, J. E. Kellon and J. E. Hutchison, *J. Am. Chem. Soc.*, 2016, **138**, 13975–13984.
61 K. Kwak, S. S. Kumar, K. Pyo and D. Lee, *ACS Nano*, 2014, **8**, 671–679.
62 A. a. Reitinger, N. a. Hutter, A. Donner, M. Steenackers, O. a. Williams, M. Stutzmann, R. Jordan and J. a. Garrido, *Adv. Funct. Mater.*, 2013, **23**, 2979–2986.
63 K.-Y. Hwa and B. Subramani, *Biosens. Bioelectron.*, 2014, **62**, 127–33.
64 S. K. Krishnan, E. Prokhorov, D. Bahena, R. Esparza and M. Meyyappan, *ACS Omega*, 2017, **2**, 1896–1904.

View Article Online
DOI: 10.1039/C7TB01346A

Table of Content Graphic

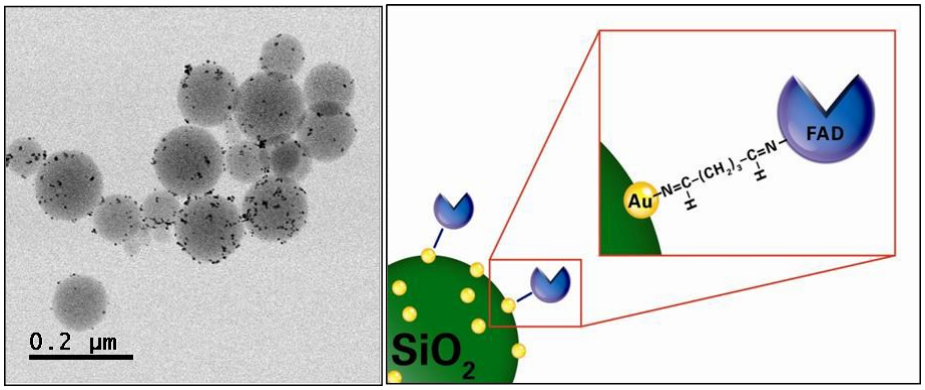

Synthesis of AuNPs–supported nanosilica mediated by deep eutectic solvent (DES) for efficient immobilization of glucose oxidase (GOx) and enhanced direct electron transfer in enzymatic biosensor.